Direct Flux-and-Torque Vector Control with Active Torque Ripple Minimization

Direct Flux-and-Torque Vector Control with Active Torque Ripple Minimization

Andrei Bojoi, *DENERG*, *Politecnico di Torino*, Torino, Italy, andrei.bojoi@polito.it
Paolo Pescetto, *DENERG*, *Politecnico di Torino*, Torino, Italy, paolo.pescetto@polito.it
Fausto Stella, *DENERG*, *Politecnico di Torino*, Torino, Italy, fausto.stella@polito.it
Simone Ferrari, *DENERG*, *Politecnico di Torino*, Torino, Italy, simone.ferrari@polito.it
Gianmario Pellegrino, *DENERG*, *Politecnico di Torino*, Torino,Italy, gianmario.pellegrino@polito.it

***Abstract*—The paper presents a simple and effective direct flux and torque control strategy for the active minimization of torque ripple in Permanent Magnet synchronous motor drives. The observed stator flux amplitude and the estimated electromagnetic torque are directly controlled, and the torque feedback is estimated through a pre-determined 3D Look-Up-Table having the (d, q) current components and the measured rotor phase angle θ as inputs. The torque LUT used in the paper was obtained via dedicated preliminary experimental tests, but other methods for its determination exist, including Finite Element Analysis where possible, and manipulation of the flux d, q linkage characteristics. Simulation and experimental results are provided for a $10kW$ Permanent Magnet Synchronous Motor to demonstrate the validity of the proposed torque control strategy.**

I. Introduction

***Index Terms*—Torque ripple, Space harmonics, $dq\theta$ model, Instantaneous Torque Control, Synchronous motor drives**

Torque ripple minimization in Permanent Magnet (PM), Synchronous Reluctance (SyR) and Switched Reluctance (SR) [1] motor drives has been widely investigated in the literature over the last 20-plus years. The magnetic field space harmonics produce flux linkage and torque undulations which can be problematic in those applications requiring low-speed operation and/or position control. This is even more critical for sensorless applications [2], [3], where space harmonics of excessive amplitude harm the position estimation and the overall control stability. In addition, torque ripple contributes to acoustic noise and vibrations of the driveline. Therefore, active torque ripple suppression is relevant whenever the electric motor does not comply with the application requirements.

Limited to 3-phase PMSM drives with distributed windings, flux linkage space harmonics exist in the dq rotor reference frame at frequencies multiples of 6 with respect to the electrical fundamental frequency. This, in the absence of manufacturing asymmetries. Torque ripple and cogging torque usually have a main harmonic order at Q_s in one mechanical revolution, being Q_s the stator number of slots (again multiple of 6), or Q_s/p with respect to the fundamental frequency, where p is the number of pole pairs.

The torque ripple is commonly minimized at the motor design stage by torque ripple optimization [4]–[6], skewing [7], [8] or asymmetric poles [9], [10]. Whatever the suppression method, torque ripple reduction implies a tradeoff with average torque production.

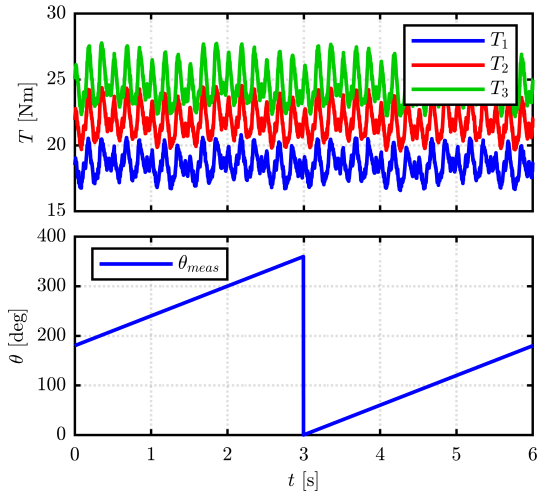

Fig. 1: Torque ripple identification for three dq points: $\boldsymbol{i_{dq,1}} = [17.5; 17.5]$, $\boldsymbol{i_{dq,2}} = [22.5; 17.5]$, $\boldsymbol{i_{dq,3}} = [27.5; 17.5]$. Top: measured torque T. Bottom: rotor electrical position θ

A feasible alternative to a minimum-torque motor design is the active suppression of the torque ripple by dedicated torque control algorithms. The control strategies found in the literature can be classified into the three main categories [11]: current profiling, speed noise cancellation and Instantaneous Direct Torque Control. Current profiling [12] refers to dq current vector control and consists of torque harmonic cancellation by means of properly distorted current trajectories on varying the torque reference and rotor position, computed offline by means of Finite Element Analysis (FEA). If a sinusoidal current supply produces torque ripple, a distorted phase current can, in principle, cancel the harmonic torque components. The computed current harmonic distortion is added to the reference signals of the current regulators. The main challenge is the cumbersome preliminary computation of the appropriate current reference signals. Other downsides are the FEA model's uncertain accuracy in the absence of experimental calibration, and uncertain availability, and the need

for a high bandwidth of response of the current regulators. In [13] a fuzzy-logic torque control is implemented, where torque ripple is minimized using the oscillations of measured speed as control feedback. However, the measurement of speed oscillations requires a position transducer with very high resolution and high dynamic of response.

In the Instantaneous Direct Torque Control schemes a flux and torque observer estimates the torque on varying the rotor position, and uses such torque estimate in a closed loop torque control. In [14] a Dead-Beat Direct Torque and Flux Control (DB-DTFC) is utilized for a Synchronous Reluctance Machine, where the feedback torque is real-time estimated including the position derivative of the magnetic coenergy. The results show partial torque compensation and the understanding of the authors is that the flux-observer is incapable of representing the flux linkage harmonic content with the needed bandwidth. In [15] an adaptive current control is implemented, where the torque of a PMSM is online estimated from the 6^{th} and the 12^{th} flux linkage harmonics, retrieved through the back-EMF integration. Besides the mathematical model being computationally non-trivial, it is also sensitive to parameter errors and limited to a finite number of flux harmonics. In [16], harmonic effects are treated as parameter uncertainties and an adaptive internal model is used to compensate for such uncertainties. The method shows good performance for a surface-mounted PM synchronous test motor with a dominant 6th harmonic torque ripple. In [17], [18], torque ripple minimization is achieved through Torque Predictive Control, by respectively varying the time duration of the applied voltage vector and by using Extended-Control-Set, i.e. more virtual vectors are used in addition to the eight inverter voltage vectors.

In this paper, a novel Instantaneous Direct Torque control strategy is proposed based on Direct Flux and Torque Vector Control. Flux amplitude and torque are controlled by two PI regulators, with no need for predefined current trajectories or cumbersome manipulation of the machine under control model. The torque feedback is estimated based on a 3D Look-Up-Table, function of the dq current components and the rotor phase angle θ, therefore including the torque ripple component at any operating point. The 3D torque LUT was directly measured on the motor under test, as described in the paper.

The paper is organized as follows. Section II presents the $dq\theta$ model approach and the torque ripple map identification test. The proposed control scheme is described in Section III. Simulation and experimental results are given in Sections IV and V respectively, while Section VI concludes the paper.

II. Motor Modelling with Space Harmonics

A. $dq\theta$ motor model

Generally, the non-linear magnetic characteristics, including saturation and cross-saturation effects, are represented by the saturation curves or flux maps $\boldsymbol{\lambda}_{dq}(\boldsymbol{i}_{dq})$. This is called the fundamental saturation model, where the flux linkage values refer to purely sinusoidal current supply and their dq values are averaged over one electrical (or mechanical) period for extracting the fundamental component. Neglecting harmonic effects, the average electromagnetic torque T_{dq} can be derived from the cross product of the current and flux linkage fundamental vectors:

TABLE I: Ratings of the motor under test

Number of pole pairs	2	
Number of slots	36	
Nominal DC-link voltage	300	[V]
Max Current	44	$[A_{pk}]$
Nominal Torque	18	[Nm]
Max torque	43	[Nm]
Nominal speed	2500	[rpm]
Max speed	9000	[rpm]

$$T_{dq} = \frac{3p}{2} \cdot \left(\boldsymbol{i}_{dq}^{T} \cdot \boldsymbol{J} \cdot \boldsymbol{\lambda}_{dq} \right) \tag{1}$$

where p is the number of pole pairs and $\boldsymbol{J} = \left[\begin{smallmatrix} 0 & -1 \\ 1 & 0 \end{smallmatrix}\right]$. The flux maps can be either FEA computed or experimentally identified through a standard constant-speed procedure [19] which is generally preferred for its higher accuracy and wider availability, as the FEA model of the motor is exclusively held by the motor manufacturer. If the space harmonics effects are to be included, the $dq\theta$ flux maps $\boldsymbol{\lambda}_{dq}(i_{dq}, \theta)$ approach is suggested, as described in [20]. The $dq\theta$ maps are an extension of the dq model, where the flux linkage and torque are also functions of the electrical rotor position θ:

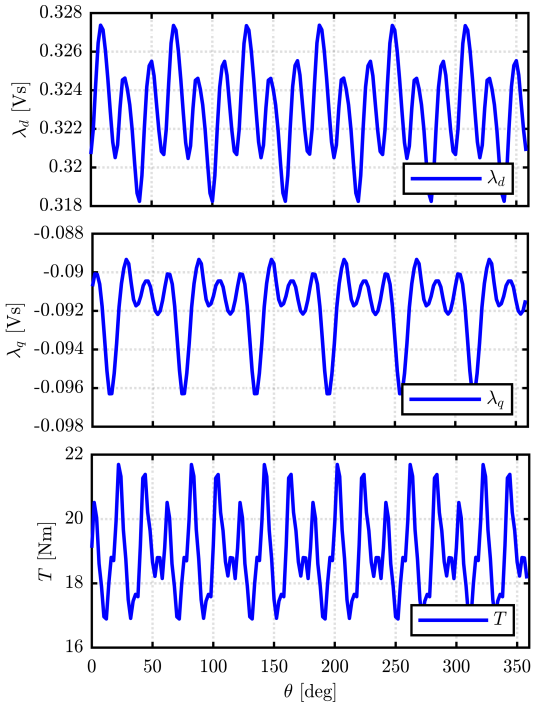

Fig. 2: Top to Bottom: FEA evaluated d-axis λ_d, q-axis λ_q flux linkages and torque T, function of electrical angle θ

$$\lambda_d = \lambda_d(i_d, i_q, \theta) \tag{2a}$$
$$\lambda_d = \lambda_d(i_d, i_q, \theta) \tag{2b}$$
$$T = T(i_d, i_q, \theta) \tag{2c}$$

In the dq maps, the rotor position information is lost when the λ_{dq} fluxes are averaged over the electrical period. This approach covers all space harmonics effect on torque and flux linkages, including back-EMF undulation. Such effects are pointed out in Fig. 2, showing the λ_d, λ_q and torque waveforms of a 10kW PM-Assisted-Synchronous-Reluctance Machine. The ratings of the reference machine are listed in Tab. I. This reference PMSM is used for simulation and experimental validation of the proposed technique, as reported in Sections IV and V.

In principle, the $dq\theta$ torque map can be derived by manipulation of the $dq\theta$ flux maps. In particular, the instantaneous electromagnetic torque can be computed as:

$$T(i_d, i_q, \theta) = \frac{3p}{2} \cdot \left(\boldsymbol{i}_{dq}^T \cdot \boldsymbol{J} \cdot \boldsymbol{\lambda}_{dq} + \frac{\partial W'}{\partial \theta} \right) \tag{3}$$

where $W'(i_d, i_q, \theta)$ is the magnetic co-energy. Being a conserved quantity, the co-energy does not depend on the path of the integral; it can be thus expressed as the sum of the d and q axis components, called $W'_d(i_d, 0, \theta)$ and $W'_q(i_d, i_q, \theta)$ respectively, assuming that the d-axis is magnetized first and then the q-axis:

$$W'(i_d, i_q, \theta) = W'_d(i_d, 0, \theta) + W'_q(i_d, i_q, \theta) \tag{4}$$

$$W'_d(i_d, 0, \theta) = \int_0^{i_d} \lambda_q(x, 0, \theta) dx \tag{5a}$$
$$W'_q(i_d, i_q, \theta) = \int_0^{i_q} \lambda_q(i_d, x, \theta) dx \tag{5b}$$

The co-energy based derivation requires that experimental $dq\theta$ flux maps are available at high resolution in the θ dimension, and their appropriate manipulation. This is the subject of future work. As said, in this paper the 3D torque LUT was obtained by direct measurement of the torque waveform across the i_{dq} domain.

B. Torque map measurement

The proposed torque control technique uses the measured $dq\theta$ torque map of the motor under test. The method for the direct measurement of the machine torque ripple is described in [9]. A dedicated low speed test bench, represented in Fig. 3, includes a speed-controlled driving machine mechanically coupled with the motor under test (MUT) through a gearbox with a high ratio and a torquemeter (T40B 100Nm by HBM). This permits imposing a very low and stable speed at the MUT shaft, and at the same time suppresses any ripple of the driving machine from propagating to the torque measurement. The MUT is current controlled, with the current vector systematically exploring the dq current plane along a regular grid of points. In each $\boldsymbol{i}_{dq}$ measurement point, the current is maintained for one mechanical revolution, and the torque waveform is measured by the torque meter at high sampling rate, together with the rotor position. The shaft rotates at 10 rpm, corresponding to 6 s per revolution. The obtained data is then post-processed for the 3D torque ripple map computation. The i_d, i_q current grid covers the range $0A - 35A$, with current steps of $2.5A$. An example or results is given in Fig.1, representing the measured torque and electrical position for grid points $i_{dq,1} = [17.5; 17.5]$, $i_{dq,2} = [22.5; 17.5]$ and $i_{dq,3} = [27.5; 17.5]$.

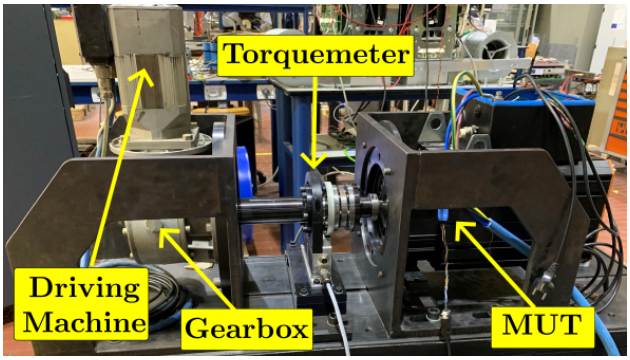

Fig. 3: Workbench for torque ripple identification and experimental validation.

The torque ripple measurement described in [9] requires a dedicated test rig, which includes a torque meter and a gearbox, and accurate sinusoidal current control. An alternative procedure is to compute the torque ripple starting from the $dq\theta$ flux undulation, which can be measured under sinusoidal [21] or even distorted [22], current waveforms. In this case, the torque maps are computed from (3)-(5). This approach is the scope of future works.

III. Proposed Control Strategy

A. Background of Direct Flux Vector Control

The proposed control algorithm is based on Direct Flux Vector Control (DFVC) [23], which is briefly described here. DFVC operates in the (d_s, q_s) stator flux coordinates, with d_s aligned with the stator flux vector and θ_s being the phase of the observed flux linkage vector with respect to the stator α axis. The controlled variables are the flux amplitude λ and the i_{qs} current component, which is perpendicular to the flux vector. Both these variables are closed loop imposed by two dedicated PI regulators.

In stator flux coordinates, the voltage vector $\boldsymbol{v}_{dsqs}$ and the fundamental torque T_{dq} can be written as:

$$\begin{cases} v_{ds} = & R_s i_{ds} + \frac{d\lambda}{dt} \\ v_{qs} = & R_s i_{qs} + \lambda \cdot \left(\omega + \frac{d\delta}{dt}\right) \end{cases} \tag{6}$$

$$T_{dq} = \frac{3}{2} \cdot p \cdot \lambda \cdot i_{qs} \tag{7}$$

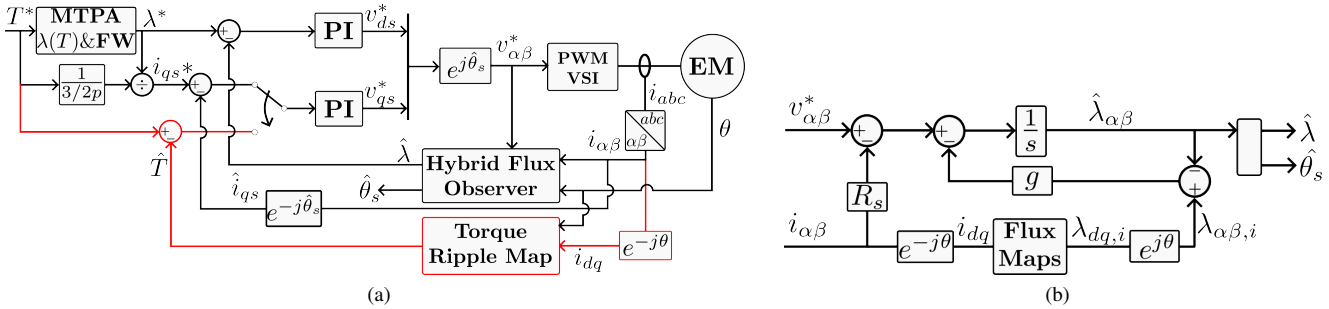

Fig. 4: (a) Block diagram of the control scheme; (b) hybrid flux observer.

The flux reference λ^* is retrieved by the Maximum Torque Per Ampere (MTPA), and saturated to λ_{max} to implement the field weakening (FW) operation.

$$\lambda_{max} = \frac{\sqrt{\frac{v_{dc}^2}{3} - R_s i_{ds}^2} - R_s |i_{qs}|}{|\omega|} \approx \frac{\frac{v_{dc}}{\sqrt{3}} - R_s |i_{qs}|}{|\omega|} \tag{8}$$

The reference current i_{qs}^* is retrieved by reversing the fundamental torque equation in (7). The flux linkage vector, its amplitude and phase θ_s are estimated by means of a Hybrid Flux Observer (HFO), represented in Fig. 4b. The HFO merges the flux estimation based on the measured current vector and 2D flux maps LUTs (current model) with the back-EMF integration (voltage model).

B. Proposed DTFC with active torque ripple cancellation

The proposed control scheme for the torque ripple cancellation is depicted in Fig. 4a. With respect to the canonical DFVC, the HFO structure and the flux control loops are maintained, but the second controlled variable is the instantaneous motor torque, closed-loop controlled by means of the PI regulator. The feedback torque estimate is obtained by the 3D torque map, or $dq\theta$ torque estimate, which outputs the instantaneous machine torque computed with a tri-linear interpolation in the (i_d, i_q, θ) domain.

Given a constant reference torque, the closed loop PI torque control tends to cancel the torque error, i.e. to force the torque estimate $\hat{T}$ to be equal to the (constant) T^*. Provided that the feedback $\hat{T}$ contains the $dq\theta$ harmonics, the torque undulation is suppressed. It should be noted that, due to the space harmonics in the machine, imposing a constant instantaneous torque corresponds to non-sinusoidal phase currents. Anyway, differently from the current profiling methods such as [12], the appropriate current distortion is not to be computed; it comes as the result of the closed loop torque control.

It should be noted that the flux control loop is unchanged with respect to the DFVC. This permits to impose the operating point on the MTPA, and to implement flux weakening control again through the limitation of the flux amplitude reference $\lambda^* < \lambda max$.

The calibration of the two PI regulators is presented in (9). The calibration of the flux loop is retrieved from (6), with the proportional gain equal to the desired bandwidth, while the torque loop is calibrated based on (7):

$$k_{p,\lambda} = \omega_{b,\lambda} \qquad k_{i,\lambda} \ll k_{p,\lambda} \tag{9a}$$

$$k_{p,T} = \frac{1}{\frac{3}{2} p \lambda_n} \cdot \omega_{b,T} \cdot l_q \qquad k_{i,T} \ll k_{p,T}\omega_{b,T} \tag{9b}$$

where $\omega_{b,\lambda}$ and $\omega_{b,T}$ are the bandwidth for flux and torque control respectively, $k_{p,\lambda}$ and $k_{i,\lambda}$ are the proportional and integral gains of the flux PI regulator, $k_{p,T}$ and $k_{i,T}$ are the proportional and integral gains of the torque regulator, λ_n is the nominal flux amplitude and l_q is the d-axis incremental inductance. For simplicity, $\omega_{b,\lambda} = \omega_{b,T}$ can be imposed and l_q is computed in the nominal torque dq current point.

IV. Simulation Results

The proposed torque control strategy was tested in the Matlab-Simulink environment. The adopted e-drive simulation model, described in [24], is based on the $dq\theta$ approach, and accounts for PWM voltage supply, magnetic saturation and undulation in torque, flux and EMF due to space harmonics effects.

An example of simulation results is represented in Fig. 5. The MUT was torque controlled, with the reference set at $T^* = 20Nm$, while the speed is imposed at 100 rpm. The test started with the MUT controlled under DFVC. At the time $t = 0.5s$ the proposed torque ripple suppression technique was activated by acting on the switch in Fig. 4a, and the controlled variable passed from i_{qs} to $\hat{T}$. The upper plot of Fig. 5, reports the estimated torque $\hat{T}$ (red line) computed from the 3D torque map, which is well in accordance with the simulated motor torque T (blue line). As can be noted, under DFVC (i.e. $t < 0.5\ s$) the peak-to-peak torque ripple was significant ($\approx 5Nm$, oscillating between 23 and 18 Nm), while it was well regulated by the active torque ripple suppression strategy ($t > 0.5\ s$), with a residual peak-to-peak ripple lower than 0.5 Nm.

The corresponding phase currents are reported in the second subplot of Fig.5. As can be noted, the current was practically sinusoidal for $t < 0.5\ s$, demonstrating the correct DFVC implementation, while the current was distorted for $t > 0.5\ s$, in order to suppress the torque harmonics. No significant effects were seen on the estimated flux amplitude $\hat{\lambda}$, depicted in the third subplot of Fig. 5. The transition of the controlled

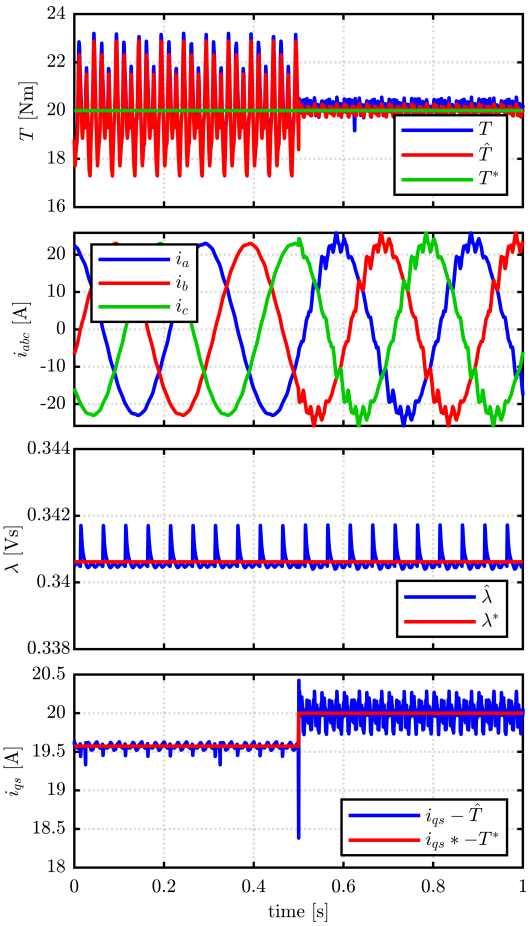

Fig. 5: Control strategy: DFVC for $t < 0.5s$ and instantaneous torque control for $t > 0.5s$. From top to bottom: Estimated $\hat{T}$, motor T and T^* reference torque; Phase currents i_{abc}; reference λ^* and observed $\hat{\lambda}$ flux amplitude; reference i_{qs}^* and feedback i_{qs} for $t < 0.5s$ and reference and feedback torque for $t > 0.5s$.

variable is represented in the last subplot of Fig. 5: for $t < 0.5$ s the reference current was computed according to (7), and the feedback was the measured i_{qs}, while the reference and feedback variables were T^* and $\hat{T}$ for $t > 0.5$ s, where the torque ripple suppression is activated.

V. Experimental results

Experimental results were obtained using the test bench presented in Fig. 3. The torquemeter permitted to measure the motor torque, denoted as T_{meas}. This measurement, although not used for control purposes, allowed the real-time monitoring of the torque at the shaft. It should be noted that the gearbox permits the suppression of the torque ripple due to the driving machine, so the measured torque undulation is only due to the MUT. The motor was supplied by a 2-level three-phase inverter operating at 10 kHz, and commanded through a dSpace control platform DS1005. The dc-link voltage was set to the rated value of 300 V.

The comparison between the DFVC with and without the proposed torque ripple suppression strategy is presented in Fig. 6. In this test, the motor was controlled at 20 Nm and the measurements were acquired for 4 electrical periods. By using the conventional DFVC, the peak-to-peak torque ripple is ≈ 4 Nm, while this value is reduced to ≈ 1.5 Nm when the minimization is activated. The introduced current distortion, trying to suppress the torque ripple, is clearly visible.

The bottom pictures in Fig. 6 present the Fast-Fourier-Trasnform (FFT) on the torque waveform. The fundamental harmonic amplitude is equal to the average average value of 20 Nm, which is out of scale in the figures. When the motor is controlled under DFVC, the predominant torque harmonics are the 6^{th}, the 12^{th} and the 18^{th}, as expected from the motor design, number of slots and FEA analysis in Fig. 2. Moreover, the adopted prototype presents a limited 2^{nd} order harmonic due to manufacturing asymmetries. The proposed torque ripple suppression was demonstrated to be effective, reducing the 6^{th} harmonic from 0.256 to 0.094 Nm, the 12^{th} harmonic from 0.539 to 0.0489 Nm and the 18^{th} harmonic from 1.086 to 0.214 Nm, while the average torque is still properly controlled at 20 Nm. The limited residual torque undulation is partially due to the measurement noise and uncertainty of the torquemeter and partially to the imperfect 3D torque LUTs.

Finally, a staircase torque reference was imposed in the test reported in Fig. 7. The torque was imposed in steps of $2Nm$, spanning from 10 to $20Nm$. As can be noticed, the torque ripple suppression strategy is effective at any load level, with similar performance. The bottom figure also reports a comparison between the two cases when the torque has reached 20 Nm, emphasizing the torque ripple reduction obtained with the proposed technique.

VI. Conclusions

This paper presents a torque control algorithm capable of actively suppressing the torque ripple in a saturated PMSM drive. The method exploits a 3D of $dq\theta$ torque LUT, to extract the instantaneous torque waveform function of the dq current components and rotor position. The identification of the torque map is performed by means of a dedicated test rig, equipped with a torquemeter. The control algorithm relies on two PI regulators controlling the flux amplitude and the instantaneous torque estimate. There is no need for time-consuming computation of current trajectories or more complicated control algorithms. Simulation results provide excellent results, with total suppression of the torque undulations. Experimental validation shows a reduction of the amplitude of the machine main harmonics, thus the 6^{th},12^{th} and 18^{th}. Future work will investigate the identification of torque ripple without a dedicated test bench and a torque sensor. Also the medium-high region will be analyzed.

Acknowledgment

The research was conducted with the support of the Power Electronics Innovation Center (PEIC) of Politecnico di Torino.

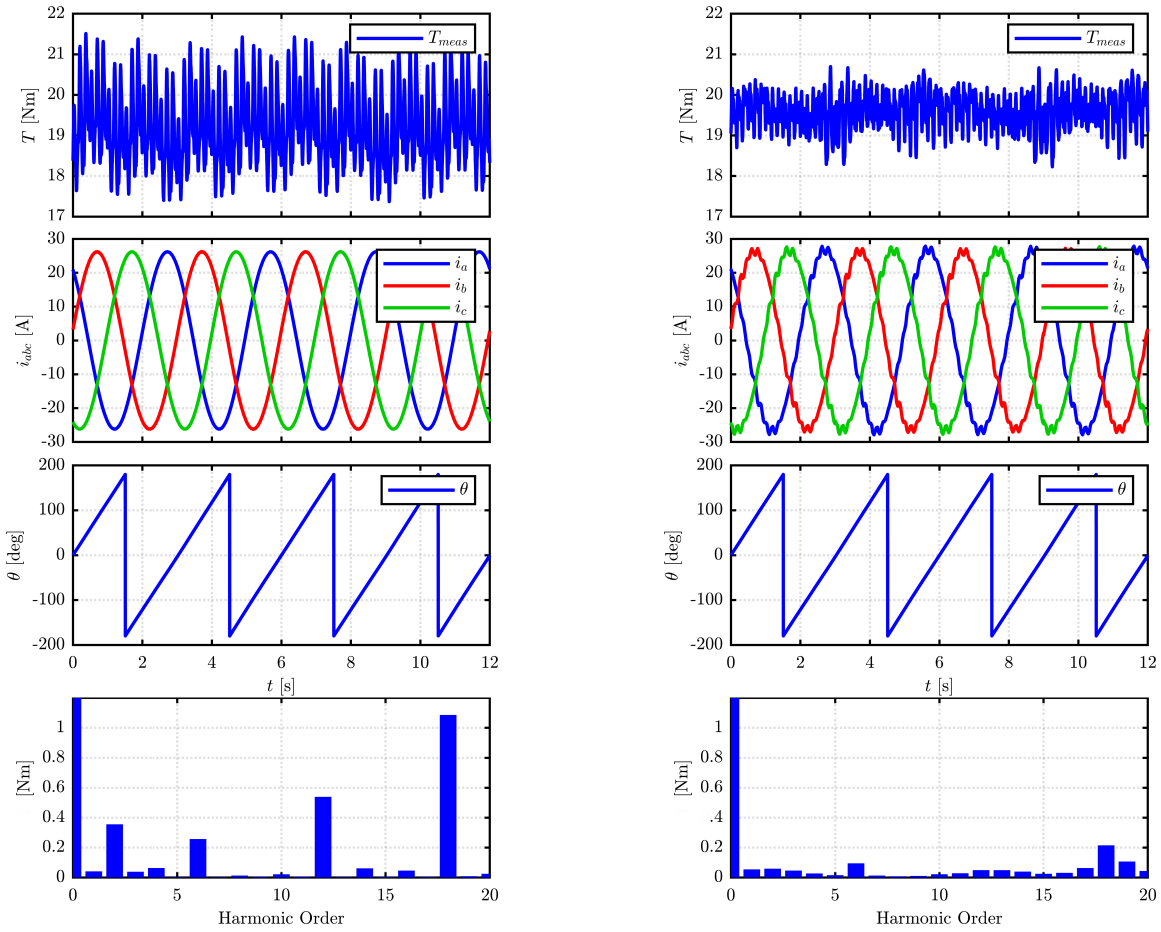

Fig. 6: From Top to Bottom: measured torque, three phase currents, electrical rotor position, Fast Fourier Transform. Left: DFVC; right DFVC with torque ripple suppression.

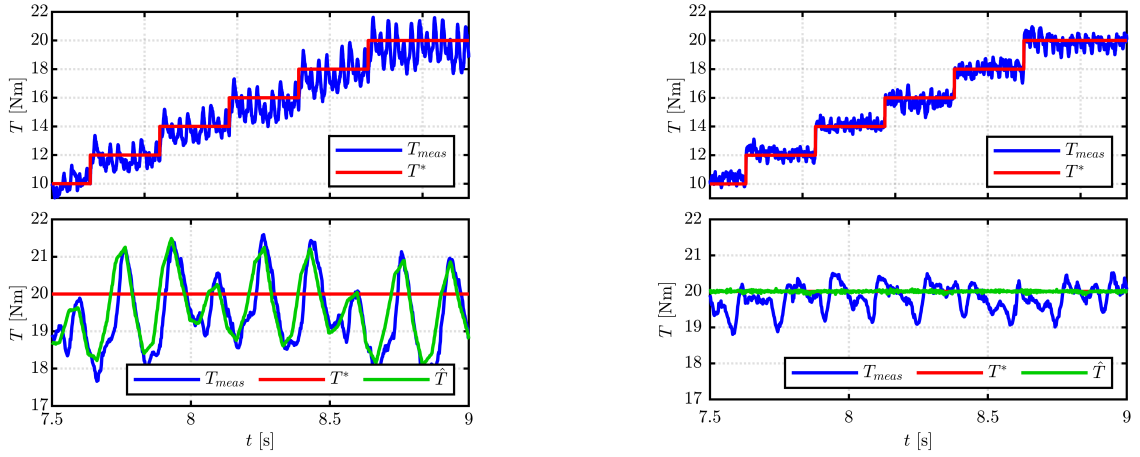

Fig. 7: Measured, estimated and reference torque. Left: DFVC; Rigth: DFVC with torque ripple suppression.

REFERENCES

[1] I. Husain, "Minimization of torque ripple in srm drives," *IEEE Transactions on Industrial Electronics*, vol. 49, no. 1, pp. 28–39, 2002.

[2] F. Stella, A. Yousefi-Talouki, S. Odhano, G. Pellegrino, and P. Zanchetta, "An accurate self-commissioning technique for matrix converters applied to sensorless control of synchronous reluctance motor drives," *IEEE Journal of Emerging and Selected Topics in Power Electronics*, vol. 7, no. 2, pp. 1342–1351, 2019.

[3] F. Stella, G. Pellegrino, E. Armando, and D. Daprà, "Advanced testing of sic power mosfet modules for electric motor drives," in *2017 IEEE International Electric Machines and Drives Conference (IEMDC)*, 2017, pp. 1–8.

[4] R.-R. Moghaddam, F. Magnussen, and C. Sadarangani, "Novel rotor design optimization of synchronous reluctance machine for low torque ripple," in *2012 XXth International Conference on Electrical Machines*, 2012, pp. 720–724.

[5] D. Wu and Z. Q. Zhu, "Design tradeoff between cogging torque and torque ripple in fractional slot surface-mounted permanent magnet machines," *IEEE Transactions on Magnetics*, vol. 51, no. 11, pp. 1–4, 2015.

[6] W. Zhao, F. Zhao, T. A. Lipo, and B.-I. Kwon, "Optimal design of a novel v-type interior permanent magnet motor with assisted barriers for the improvement of torque characteristics," *IEEE Transactions on Magnetics*, vol. 50, no. 11, pp. 1–4, 2014.

[7] R. Islam, I. Husain, A. Fardoun, and K. McLaughlin, "Permanent-magnet synchronous motor magnet designs with skewing for torque ripple and cogging torque reduction," *IEEE Transactions on Industry Applications*, vol. 45, no. 1, pp. 152–160, 2009.

[8] L. Jia, M. Lin, W. Le, N. Li, and Y. Kong, "Dual-skew magnet for cogging torque minimization of axial flux pmsm with segmented stator," *IEEE Transactions on Magnetics*, vol. 56, no. 2, pp. 1–6, 2020.

[9] S. Ferrari, E. Armando, and G. Pellegrino, "Torque ripple minimization of pm-assisted synchronous reluctance machines via asymmetric rotor poles," in *2019 IEEE Energy Conversion Congress and Exposition (ECCE)*, 2019, pp. 4895–4902.

[10] J. Qi, Z. Zhu, L. Yan, G. Jewell, C. Gan, Y. Ren, S. Brockway, and C. Hilton, "Suppression of torque ripple for consequent pole pm machine by asymmetric pole shaping method," in *2021 IEEE International Electric Machines Drives Conference (IEMDC)*, 2021, pp. 1–7.

[11] G. Velmurugan, S. Bozhko, and T. Yang, "A review of torque ripple minimization techniques in switched reluctance machine," in *2018 IEEE International Conference on Electrical Systems for Aircraft, Railway, Ship Propulsion and Road Vehicles International Transportation Electrification Conference (ESARS-ITEC)*, 2018, pp. 1–6.

[12] G.-H. Lee, S.-I. Kim, J.-P. Hong, and J.-H. Bahn, "Torque ripple reduction of interior permanent magnet synchronous motor using harmonic injected current," *IEEE Transactions on Magnetics*, vol. 44, no. 6, pp. 1582–1585, 2008.

[13] G. Feng, C. Lai, and N. C. Kar, "A closed-loop fuzzy-logic-based current controller for pmsm torque ripple minimization using the magnitude of speed harmonic as the feedback control signal," *IEEE Transactions on Industrial Electronics*, vol. 64, no. 4, pp. 2642–2653, 2017.

[14] M. Saur, D. E. Gaona Erazo, J. Zdravkovic, B. Lehner, D. Gerling, and R. D. Lorenz, "Minimizing torque ripple of highly saturated salient pole synchronous machines by applying db-dtfc," *IEEE Transactions on Industry Applications*, vol. 53, no. 4, pp. 3643–3651, 2017.

[15] V. Petrovic, R. Ortega, A. Stankovic, and G. Tadmor, "Design and implementation of an adaptive controller for torque ripple minimization in pm synchronous motors," *IEEE Transactions on Power Electronics*, vol. 15, no. 5, pp. 871–880, 2000.

[16] Y. A.-R. I. Mohamed and E. F. El-Saadany, "A current control scheme with an adaptive internal model for torque ripple minimization and robust current regulation in pmsm drive systems," *IEEE Transactions on Energy Conversion*, vol. 23, no. 1, pp. 92–100, 2008.

[17] Y. Cho, K.-B. Lee, J.-H. Song, and Y. I. Lee, "Torque-ripple minimization and fast dynamic scheme for torque predictive control of permanent-magnet synchronous motors," *IEEE Transactions on Power Electronics*, vol. 30, no. 4, pp. 2182–2190, 2015.

[18] Z. Zhou, C. Xia, Y. Yan, Z. Wang, and T. Shi, "Torque ripple minimization of predictive torque control for pmsm with extended control set," *IEEE Transactions on Industrial Electronics*, vol. 64, no. 9, pp. 6930–6939, 2017.

[19] E. Armando, R. I. Bojoi, P. Guglielmi, G. Pellegrino, and M. Pastorelli, "Experimental identification of the magnetic model of synchronous machines," *IEEE Transactions on Industry Applications*, vol. 49, no. 5, pp. 2116–2125, 2013.

[20] S. Ferrari, G. Dilevrano, P. Ragazzo, and G. Pellegrino, "The dq-theta flux map model of synchronous machines," in *2021 IEEE Energy Conversion Congress and Exposition (ECCE)*, 2021, pp. 3716–3723.

[21] J. Lee, Y. C. Kwon, and S. K. Sul, "Identification of IPMSM Flux-Linkage Map for High-Accuracy Simulation of IPMSM Drives," *IEEE Transactions on Power Electronics*, 2021.

[22] A. Varatharajan, P. Pescetto, S. Ferrari, and G. Pellegrino, "Flux maps spatial harmonic modeling and measurement in synchronous reluctance motors," in *2023 IEEE Energy Conversion Congress and Exposition (ECCE)*.

[23] G. Pellegrino, R. I. Bojoi, and P. Guglielmi, "Unified direct-flux vector control for ac motor drives," *IEEE Transactions on Industry Applications*, vol. 47, no. 5, pp. 2093–2102, 2011.

[24] A. Bojoi, S. Ferrari, P. Pescetto, and G. Pellegrino, "Advanced circuital model for e-drive simulation, including harmonic effects and fault scenarios," in *PCIM Europe 2023; International Exhibition and Conference for Power Electronics, Intelligent Motion, Renewable Energy and Energy Management*, 2023, pp. 1–10.